PCCP

PAPER

View Article Online
View Journal | View Issue

Cite this: *Phys. Chem. Chem. Phys.*, 2024, **26**, 15902

O_2 activation by subnanometer Re–Pt clusters supported on TiO_2(110): exploring adsorption sites†

Andrés Álvarez-García,[a] Luis M. Molina[b] and Ignacio L. Garzón*[a]

Received 14th March 2024,
Accepted 15th May 2024

DOI: 10.1039/d4cp01118j

rsc.li/pccp

Activation of O_2 by subnanometer metal clusters is a fundamental step in the reactivity and oxidation processes of single-cluster catalysts. In this work, we examine the adsorption and dissociation of O_2 on Re_nPt_m ($n + m = 5$) clusters supported on rutile TiO_2(110) using DFT calculations. The adhesion energies of Re_nPt_m clusters on the support are high, indicating significant stability of the supported clusters. Furthermore, the bimetallic Re–Pt clusters attach to the surface through the Re atoms. The oxygen molecule was adsorbed on three sites of the supported systems: the metal cluster, the surface, and the interface. At the metal cluster site, the O_2 molecule binds strongly to Re_nPt_m clusters, especially on the Re-rich clusters. O_2 activation occurs by charge transfer from the metal atoms to the molecule. The dissociation of O_2 on the Re_nPt_m clusters is an exothermic process with low barriers. As a result, subnanometer Re–Pt clusters can be susceptible to oxidation. Similar results are obtained at the metal-support interface, where both the surface and cluster transfer charge to O_2. To surface sites, molecular oxygen is adsorbed onto the Ti_{5c} atoms with moderate adsorption energies. The polarons, which are produced by the interaction between the metal cluster and the surface, participate in the activation of the molecule. However, dissociating O_2 in these sites is challenging due to the endothermic nature of the process and the high energy barriers involved. Our findings provide novel insights into the reactivity of supported clusters, specifically regarding the O_2 activation by Re–Pt clusters on rutile TiO_2(110).

1 Introduction

Supported metal clusters (SMCs) represent a category of heterogeneous catalysts comprising metal clusters attached to solid supports, such as metal oxides.[1] Re–Pt clusters supported on titania are employed as catalysts for the water–gas shift reaction[2] and CO oxidation.[3,4] Rhenium has a variety of valence states and higher oxophilicity than other noble metals (Pt, Ir), which may enhance catalytic multifunctionality.[5] The utilization of Re–Pt catalysts leads to an economical process because of their extended catalyst lifespan and high yield of desired products.[6] The bimetallic system of Re–Pt exhibits unique properties that differ from those of pure Pt and pure Re in catalytic reactions.[3] The catalyst containing Re–Pt/TiO_2 exhibits higher activity than the pure Pt/TiO_2 catalyst for the water gas shift (WGS) reaction.[7] The interaction between oxygen and Re–Pt bimetallic clusters is relevant in the aforementioned reactions because PtO_x and ReO_x can act as promoters or inhibitors.[8] The activation of O_2 is a pivotal step in oxidation processes, resulting in the creation of more reactive species, such as superoxo, peroxo, and atomic oxygen.[9,10] Several factors can influence the activation of O_2, including the support type, cluster size, and interface perimeter.[11–13] Additionally, metals featuring a low O_2 dissociation barrier exhibit a tendency to adsorb O_2 and O strongly, rendering them susceptible to oxidation.[14]

Recently, there has been an increasing interest in subnanometer clusters as single-cluster catalysts (SCCs). Small metal clusters, typically composed of fewer than 20 atoms (with a diameter of less than 1 nm), are supported on suitable matrices to form SCCs.[15] They are an intermediate size between traditional metal nanoparticles and single-atom catalysts (SACs).[16–18] Subnanometer metal clusters exhibit unique physicochemical

---

[a] *Instituto de Física, Universidad Nacional Autónoma de México, Apartado Postal 20-364, Ciudad de México 01000, Mexico. E-mail: garzon@fisica.unam.mx*
[b] *Departamento de Física Teórica, Atómica y Optica, Universidad de Valladolid, E-47011 Valladolid, Spain*

† Electronic supplementary information (ESI) available: Table S1 presents the Bader charge analysis of supported Re_nPt_m clusters on TiO_2(110), while Table S3 displays this analysis for O_2 activation on the supported clusters. Table S2 shows the structural and energetic parameters for O_2 adsorption on the surface site in the presence of supported Re_nPt_m clusters. The most stable structures of gas-phase clusters are displayed in Fig. S1. The lowest energy isomers are displayed in Fig. S2 and S3. The most stable structures for O_2 dissociation on Re_nPt_m supported clusters are shown in Fig. S4. Finally, the structures for dissociative adsorption of O_2 on the Re–Ti interface are presented in Fig. S5. See DOI: **https://doi.org/10.1039/d4cp01118j**

properties due to quantum confinement effects.[19] Controlling the size and arrangement of SCCs with atomic precision is crucial for adjusting the activity and stability of clusters in different catalytic applications.[20] Furthermore, the precise control of subnanometer clusters can result in the formation of bimetallic catalysts, such as Au_4Pt_2[21] and Rh_1Co_3[22] clusters.

The stability of subnanometer clusters is maintained by the metal-support interactions, as well as the low kinetic energy deposition.[23] Interactions between highly reactive metals (with incomplete d-shells), such as Re, and reducible oxides, such as titania, can stabilize supported metal clusters composed of only a few atoms.[24–26] Ultra-small Re clusters (size = 2–13 atoms) were deposited on graphene and studied by high annular dark-field scanning transmission electron microscopy (HAADF-STEM), where Re clusters presented 3D structures above four-atom size.[27] Subnanometer Pt_n ($n = 4, 7–10, 15$) clusters were deposited on the $TiO_2(110)$ surface and imaged at atomic resolution using an ultrahigh vacuum scanning tunneling microscope.[28] The Pt_7 cluster on $TiO_2(110)$ exhibits catalytic activity in CO oxidation, where reduction conditions can play a significant role in CO_2 production.[29] While there are no reports of subnanometer-scale Re–Pt clusters, they have been studied in larger clusters.[7] In our previous work, we analyzed the structure of Re–Pt clusters in both the gas phase and supported on the MgO(100) surface. Our findings revealed a transition from a 2D to a 3D configuration at size five.[30] In addition, five-atom size clusters allow for the exploration of 3D configurations, with atoms directly interacting with the substrate and others forming a second layer.

The Cu_5 cluster has been synthesized with atomic precision and exhibits stability to ultraviolet radiation, temperature, and pH, rendering it an ideal model for the study of polarons in oxide-supported clusters.[31] Oxides can serve as inert matrices for dispersing metal nanoparticles or as catalysts themselves. The reducible oxides, such as TiO_2, CeO_2, and Fe_2O_3, are capable of exchanging oxygen atoms, making them effective in oxidation reactions.[32–34] In particular, the reactivity of rutile $TiO_2(110)$ surface for O_2 adsorption and dissociation has been studied.[35] Oxygen vacancies (O_v) on the $TiO_2(110)$ surface act as a source of excess electrons, leading to the dissociation of O_2.[36,37] This excess of electrons can also be achieved by charge transfer from metal clusters with low resistance to electron donation.[38–40] Specifically, Cu_5 and Ag_5 clusters donate electrons to the support, inducing the formation of one or two polarons.[41–43] The excess charge is located in the 3d states of Ti, which causes a reduction of its oxidation state from Ti^{4+} to Ti^{3+}. Therefore, the study of subnanometer clusters of five-atom size supported on titania is of significant interest due to their computational simplicity, preference for 3D conformations, and the existing background on this topic.

Modeling subnanometer clusters supported on metal oxides is challenging due to their structural intricacies.[44] To address this issue, utilizing global optimization algorithms such as Basin-Hopping[45] or Genetic Algorithms[46] in conjunction with Density Functional Theory (DFT) may be advantageous. In this manuscript, we present an extensive study of the structure of subnanometer Re_nPt_m ($n + m = 5$) clusters supported on the rutile $TiO_2(110)$ surface, evaluating the O_2 adsorption and activation on these bimetallic clusters as a function of their relative Re–Pt content. The configuration space of the supported clusters is explored using the Basin-Hopping DFT algorithm. Then, the most stable isomers were selected for a complete study of O_2 adsorption at all the possible binding sites: the metal cluster, the $TiO_2(110)$ surface away from the supported cluster, and the interfacial region around the cluster. The O–O bond activation is evaluated by various structural (bond length, O–O stretching frequency) and electronic parameters (spin magnetic moment, Bader charges, and density of states). Finally, the dissociation of O_2 is also studied using the Nudged Elastic Band (NEB) approach to obtain the activation barriers for this process.

2 Computational details

The structures of the gas-phase Pt_nRe_m ($n + m = 5$) clusters were obtained from our previous study,[30] where we performed a global optimization using the Basin-Hopping DFT (BH-DFT) algorithm coupled to VASP (ESI†). The $TiO_2(110)$ surface was constructed using a 4 × 2 slab with four trilayers, with the two bottom trilayers fixed to their positions in the bulk during relaxations. The vacuum in the z-direction was 20 Å, and the neighboring images in the horizontal direction were separated by at least 8 Å. A dipole correction perpendicular to the supercell is applied to the total energy. The search for the most stable structures of Pt_nRe_m ($n + m = 5$) clusters supported on $TiO_2(110)$ was performed using the BH-DFT algorithm with 50 Monte Carlo steps.

DFT calculations were performed in the VASP code[47] employing the PBE functional[48] and the projector augmented wave (PAW) potentials.[49,50] The cutoff energy for the plane-wave basis set was 400 eV. Ti(3s, 3p, 3d, 4s), O(2s, 2p), Pt(5d, 6s), and Re(5d, 6s) electrons were treated explicitly as valence. For titanium, the DFT+U formalism[51] was used to describe the highly localized d-electrons,[52] with the parameter for the Ti(3d) level set to 4.5 eV. The evaluation of the reducibility of the surface was performed by analyzing the spin magnetic moment and spin density of the system atoms. The convergence criteria of the electronic energy of the self-consistent field (SCF) and the forces of the geometric relaxations were 10^{-6} eV and 0.01 eV $Å^{-1}$, respectively. A single Γ point was used for integration of the Brillouin zone, since the large size of the unit cell already results in converged binding energies including only this single point in the calculations.

The adsorption energy for Re_nPt_m clusters (E_{ads}[cluster]) supported on $TiO_2(110)$ was calculated as[53]

$$E_{ads}[\text{cluster}] = -E[Re_nPt_m/TiO_2] + E[TiO_2] + E[Re_nPt_m]$$

where $E[Re_nPt_m/TiO_2]$, $E[Re_nPt_m]$, and $E[TiO_2]$ correspond to the total energy of the putative global minimum of the supported clusters, gas-phase clusters, and the relaxed $TiO_2(110)$ surface, respectively. The adhesion energy (E_{adh}) was calculated using a similar equation, but the energies of the gas-phase clusters and the surface were taken at a fixed geometry of the supported cluster.

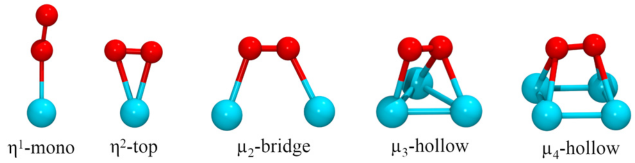

Fig. 1 Modes of adsorption of O_2 on Re_nPt_m clusters.

The adsorption of the O_2 molecule on the clusters was studied on several binding configurations, depicted in Fig. 1. The adsorption mode η^1 is the bonding of an O atom to a metal atom. In the η^2, the metal is bonded to the two atoms of the oxygen molecule. The other sites involve O_2 bonding on multiple metal atoms (μ_2, μ_3, μ_4). Previous studies have evaluated these types of adsorption sites for oxygen molecule on metal clusters.[54,55] On each case, before each structural optimization, the O_2 molecule was positioned initially 2.2 Å away from the binding site.

The adsorption energy for O_2 to the cluster, either supported or in the gas phase, ($E_{\text{ads}}[O_2]$) was calculated as

$$E_{\text{ads}}[O_2] = -E_{O_2/\text{cluster}} + E_{O_2} + E_{\text{cluster}}$$

where $E_{O_2/\text{cluster}}$, E_{O_2}, and E_{cluster} are the energies for the complex O_2-cluster, O_2 molecule in the gas-phase, and cluster, respectively. The cluster energy applies to the gas-phase or supported cluster on the $TiO_2(110)$ surface.

The charge transfer was studied through a charge density analysis with the Bader approach.[56,57] The projected of Density of States (PDOS) over each atom of the system was calculated using VASPKIT code[58] with a Gaussian broadening equal to 0.1 eV. The climbing image Nudge-elastic-band (CI-NEB) method was employed to determine the transition states for the reaction pathways of the O_2 dissociation reaction.[59] Each transition state (TS) presented only one imaginary frequency, which verifies that it is a maximum in the potential energy surface (PES). The stretching frequency of the oxygen molecule was calculated using the harmonic finite difference approximation.[60,61] We also studied how temperature affects the oxygen dissociation reaction in gas-phase clusters. We used the harmonic finite difference approximation to calculate the vibrations of the reactants (O_2 adsorption on the clusters) and the products (O_2 dissociation). The free energy at 300 K and 1 atm was determined using the post-processing code VASPKIT,[58] considering rotational, vibrational, translational, and electronic contributions.

3 Results

3.1 Structure and stability of Re_nPt_m ($n + m = 5$) clusters supported on the $TiO_2(110)$

The $TiO_2(110)$ surface has three types of sites in its topmost layer: the two-coordinate protruding oxygen (O_{2c}), the three-coordinate oxygen (O_{3c}), and the five-coordinate titanium (Ti_{5c}). The O_{2c} atoms protrude in one dimensional rows above the plane where Ti_{5c} and O_{3c} sites are located. A global optimization of Re_nPt_m ($n + m = 5$) clusters supported on $TiO_2(110)$ was performed using Basin-Hopping DFT. Fig. 2 shows the structure, absorption and adhesion energies of the global minima for each of the $Re_nPt_m/TiO_2(110)$ clusters. Although the calculations were performed with four trilayers (12 atomic layers), to improve visualization of the structure only the first trilayer of the surface is displayed. This slab model has been employed in prior investigations studying metal clusters of comparable size.[62,63]

All the clusters, excepting Re_1Pt_4, have a distorted square pyramidal shape, with its base in contact with the surface. At the global minima found, the clusters try to maximize the number of bonds between the metallic atoms in the bottom layer and the more reactive O_{2c} surface sites. In order to form stronger O–metal bonds by shortening the bond distance, the surface O_{2c} atoms suffer important lateral distortions of around 0.3–0.4 Å. The Re_1Pt_4 cluster has a very different shape, more planar, and with only three atoms in direct contact with the surface. In the case of Pt_5, our results agree with the simulations performed by Jian *et al.*,[64] who obtained the putative global minima for Pt_n ($n = 4$–8) on the rutile $TiO_2(110)$ surface, with the Pt_5 cluster also having a pyramidal square conformation.

In our previous work,[30] gas-phase Re_nPt_m ($n + m = 5$) clusters were optimized using a similar Basin-Hopping DFT algorithm (ESI,† Fig. S1). Re_3Pt_2, Re_2Pt_3, and Pt_5 clusters have planar structures, while Re_5, Re_4Pt_1, and Re_1Pt_4 clusters presented three-dimensional structures. In particular, the Re_5 cluster has a square pyramidal configuration, which does not change significantly after adsorption on the $TiO_2(110)$ surface. The high internal binding energy of the Re_5 cluster is the reason for this behavior, indicating a very strong metal–metal bond.

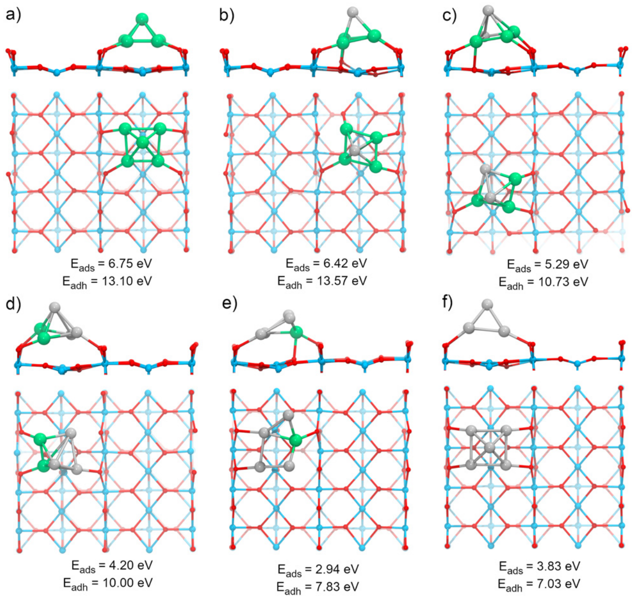

Fig. 2 Structure of Re_nPt_m ($n + m = 5$) clusters supported on $TiO_2(110)$ (Side and top views are displayed). (a) Re_5, (b) Re_4Pt_1, (c) Re_3Pt_2, (d) Re_2Pt_3, (e) Re_1Pt_4, (f) Pt_5. The adsorption (E_{ads}) and adhesion (E_{adh}) energies are displayed beneath each structure in eV. The side view only displays the final layer of the slab to aid the analysis. The colors green, gray, blue, and red represent the atoms Re, Pt, Ti, and O, respectively.

The rest of the clusters, are more fluxional, and the interaction with the substrate results in very important structural changes. For instance, the Pt_5 cluster changes from a planar house-shaped configuration to a square pyramid, which was similarly found on the $ZrO_2(101)$ surface.[65] In the ESI† (Fig. S2 and S3) we compare the global minimum found for each composition, with the first and second isomers (ISO1 and ISO2). For the clusters with a high content of Re, there are no competing isomers with the square pyramidal shape. However, as the Pt content increases, other alternate conformations have similar stabilities to the global minimum shape, as for example the ISO1 conformations for Pt_3Re_2 and Pt_4Re_1, less than 0.1 eV apart from the GM one.

Several energetic parameters have been calculated to account for the cluster–surface interaction (Fig. 2). The adsorption energy of the clusters (E_{ads}[cluster]) provides information about the stability of the cluster deposition on the substrate. In general, E_{ads}[cluster] decreases with an increasing amount of Pt in the cluster, with Re_1Pt_4 being an exception which can be attributed to the high energetic cost of the cluster distortion that takes place during adsorption; indeed, the value of the adhesion energy for this cluster is actually larger than the one for pure Pt_5,

The adhesion energy (E_{adh}), which represents the strength of the interaction between the cluster and the surface, also decreases steadily with a increasing content of Pt. In all cases, the values for E_{adh} exceed 7 eV (and reach even 13 eV for Re-rich clusters), indicating a high stability of the supported clusters. The relaxed geometries show a marked tendency towards maximizing the number of bonds between Re atoms and surface oxygen atoms; for mixed clusters, Re atoms are always in contact with the substrate, and alternate conformations with Re atoms losing contact with the support are much less stable, as Fig. S2 and S3 (ESI†) show. Comparing the values of E_{ads} or E_{adh} for Re_5 and Pt_5 (which both share the same geometric arrangement) it is clear that the intrinsic strength of O–Re bonds is approximately twice as large as the one of O–Pt bonds. The cluster–surface interaction energies for other five atom clusters supported on $TiO_2(110)$ reported in the literature are 4.50, 4.53, 5.37, and 6.87 eV for the Cu_5,[38] Ag_5,[42] Au_5,[66] and Pd_5[66] clusters, respectively. Thus, Re_nPt_m ($n + m = 5$) clusters exhibit a higher affinity for the $TiO_2(110)$ surface compared to other clusters of the same size that have been previously reported. Interestingly, the formation of strong bonds between Re and the surface O atoms is affected by the reducible character of the TiO_2 oxide; the situation changes for a non-reducible oxide as MgO, where Re-rich clusters do not fit well on the support.[30]

The Bader charge analysis shows that the Re_5 cluster donates 2.04 electrons to the surface, while Pt_5 transfers only 0.25 electrons (see data in Fig. 3). For bimetallic clusters, the charge transfer to the substrate increases steadily with the Re composition (from 0.70 to 1.74 electrons). Therefore, the stronger interaction between Re and O atoms also results in a larger degree of charge transfer towards the surface. This charge is highly localized on the Ti atoms at the surface, as evidenced by the analysis of the spin magnetic moment. In Fig. 3, we have calculated the spin density distribution and polaron formation for the supported clusters. The charge donation from clusters which contain Re results in polarons appearing on Ti^{3+} sites. In the case of the Pt_5 cluster, the spin density is localized on the metal atoms, so no polarons are formed. In contrast, for the other clusters the spin density and spin magnetic moment are localized on the surface Ti atoms. The polarons are located below or to one side of the cluster. We find that the reducibility of the $TiO_2(110)$ surface and the number of polarons formed depends on the composition of the Re_nPt_m ($n + m = 5$) clusters, ranging from one polaron (Re_1Pt_4 cluster) to three polarons (Re_5 cluster). The reduced Ti atoms exhibit a spin magnetic moment of 0.80–0.85μ_B, which serve as a parameter to characterize Ti^{3+} atoms. Interestingly, the Re_4Pt_1 cluster has one of its polarons in the subsurface, which also happens in titania with oxygen vacancies.[67] To conclude, supported Re_nPt_m ($n + m = 5$) clusters hold polarons to the surface due to the electrostatic attraction, making them more available for chemical reactions than polarons formed through vacancies.[68]

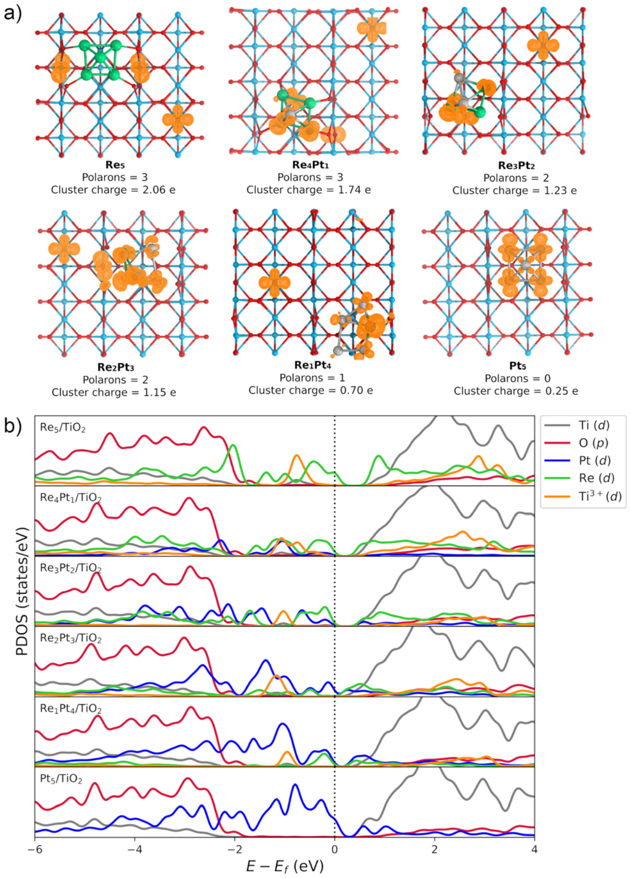

Fig. 3 Electronic properties of Re_nPt_m ($n + m = 5$) clusters supported on $TiO_2(110)$. (a) The spin density for the supported clusters. The number of polarons formed and the charge transfer from the cluster to the substrate are displayed below each structure. The spin density isosurface is shown in orange. (b) The projected density of states (PDOS) for Re_nPt_m ($n + m = 5$)/$TiO_2(110)$ clusters, where the cluster (Pt, Re) and polaron states (Ti^{3+}) have been multiplied by six to ease the observation. The Gaussian broadening used in the projection is 0.10 eV.

Fig. 3b shows the projected density of states (PDOS) of Re_nPt_m ($n + m = 5$) clusters supported on $TiO_2(110)$, where the cluster and polaron states have been multiplied by six to ease the observation. Polaron states (3d states of Ti^{3+}) are shown in yellow and are located about 1 eV below the conduction band of $TiO_2(110)$. As the number of polarons increases, the intensity of defect states is higher. The Re_5 cluster produces three polarons and has a higher intensity of Ti^{3+} states. In contrast, the supported Pt_5 cluster does not have states corresponding to a reduced Ti atom, which is consistent with the fact that they do not form polarons. Finally, the Re_4Pt_1 cluster has two orange peaks in the gap, corresponding to the surface and subsurface polarons. Furthermore, the Ti^{3+} $3d^1$ states are coupled to lattice distortions. To analyze this structural effect without interference from other interactions, we measured lattice distortions for polarons that are not in direct interaction with the cluster. This was done to avoid any interference from the metal-substrate interaction, which also produces a distortion of the surface. We found that for supported Re_5, a polaron was identified in close proximity to the cluster, exhibiting an elongation of the Ti–O bond (0.13–0.18 Å) when the oxygens were bound to the Ti cation hosting the polaron. For other clusters, polaron formation was accompanied by a lattice distortion of approximately 0.15 Å known as a phonon cloud. An alternative explanation is that the interaction between the cluster and the surface results in the reduction of Ti atoms in the substrate (from a Ti^{4+} cation to Ti^{3+}), which causes distortions in the lattice due to the increase in the ionic radius. In a similar vein, Lopez-Caballero *et al.* reported a distortion of this nature for small polarons induced by the Ag_5 cluster supported on $TiO_2(110)$.[42] Therefore, we can conclude that in the case of Pt–Re mixed clusters, the cluster–surface interaction is responsible for the formation of small polarons.[69]

3.2 Adsorption and activation of O_2 by gas-phase and supported Re_nPt_m clusters

Next, we will study the molecular adsorption and dissociation of O_2 on Re_nPt_m ($n + m = 5$ clusters, both free and supported on $TiO_2(110)$. The O_2 molecule can adsorb in three different states, as molecular oxygen (O_2), superoxo (O_2^-), or peroxo (O_2^{2-}). Calculations performed with our DFT model for the gas-phase O_2 molecule yielded a bond distance (1.23 Å,), magnetic moment ($2.0\mu_B$), and stretching vibration (1564 cm^{-1}) consistent with experiments.[70] These results support the methodology employed for the O_2 activation in the current study. The chemical adsorption of O_2 is characterized by a charge transfer from the catalyst to the oxygen molecule, forming superoxo or peroxo species. One possible way of identifying superoxo and peroxo species is to use the stretching frequency of the molecule (below about 900 cm^{-1} for peroxo and about 900 cm^{-1} for superoxo), although the boundary is not clear.[14] The assignment of a species for adsorbed O_2 depends on various electronic and structural parameters. According to experimental reports,[10] the superoxide shows an O–O bond elongation (1.35 Å), a decrease in magnetization ($1.0\mu_B$), and a shift of the stretching frequency (1100 cm^{-1}) with respect to the neutral molecule. Finally, peroxo is a non-magnetic species with more drastic O–O bond stretching (ν = 877 cm^{-1}, r = 1.48 Å).

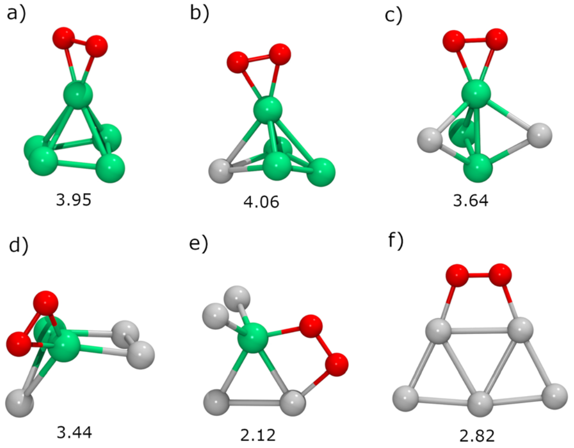

Fig. 4 The most stable structures for O_2 adsorption on gas-phase Re_nPt_m ($n + m = 5$) clusters: (a) Re_5, (b) Re_4Pt_1, (c) Re_3Pt_2, (d) Re_2Pt_3, (e) Re_1Pt_4, (f) Pt_5. The adsorption energy (E_{ads}) is displayed below each structure in eV.

In gas-phase Re_nPt_m clusters with five atoms, the adsorption energy for O_2 ranges from 2.12 to 4.06 eV, indicating a strong interaction between the molecule and the Re_nPt_m clusters (Fig. 4). In all cases, the O_2 molecule has a strong preference towards binding at the Re sites. The highest adsorption energy was obtained for clusters with significant Re content, such as Re_5, Re_4Pt_1, Re_3Pt_2, and Re_2Pt_3, which exhibit their most stable structure in the η^2-Re mode. The significant adsorption energies of O_2 suggest that desorption is unlikely, particularly in Re-rich clusters. On the other hand, Re_1Pt_4 and Pt_5 clusters prefer bridging-type adsorption (μ_2), with much lower O_2 binding energies compared to the case of Re-rich clusters. Wang *et al.* have studied the adsorption of O_2 on pure Pt clusters, with Pt_4 and Pt_6 clusters also showing a bridge-like adsorption mode for molecular O_2.[71] The O_2 molecule adsorbed on Re_nPt_m clusters has a bond length ranging from 1.40 to 1.48 Å, a stretching frequency varying from 644 to 914 cm^{-1}, and a magnetic moment close to zero (Table 1). These values suggest that, for all the gas-phase Re_nPt_m clusters, O_2 binds as a peroxo species, indicating a strong activation of the O–O bond upon molecular adsorption.

In supported Re_nPt_m ($n + m = 5$) clusters, the adsorption energy for O_2 varies from 1.37 to 3.65 eV (Fig. 5). Therefore, in all cases the clusters supported on $TiO_2(110)$ exhibit a lower adsorption energy compared to the gas-phase clusters. Several factors contribute to this decrease in reactivity, the most important being the bonding of metal atoms to the surface oxygen atoms. This surface effect is particularly clear in the cases of Re_4Pt_1 and Re_3Pt_2; for those clusters the oxygen molecule binds at Re sites which are already forming strong O–Re bonds to the substrate, and this has a high energetic cost of approximately 1.5 eV. Another effect is the transition from 2D geometries (in the unsupported case) to 3D ones for supported clusters; in the case of the Pt_5 cluster, we find a decrease of O_2 binding energy of almost 1 eV. As it happened

Table 1 The O–O bond lengths (r_{O-O}, in Å), O–O stretching frequencies (ν_{O-O}, in cm^{-1}), and magnetic moments (M_{O_2}, in μ_B) for O_2 adsorbed on the $Re_nPt_m/TiO_2(110)$ systems

Sites	Parameters	Re_5	Re_4Pt_1	Re_3Pt_2	Re_2Pt_3	Re_1Pt_4	Pt_5
Gas-phase cluster	r_{O-O}	1.46	1.47	1.48	1.47	1.48	1.40
	ν_{O-O}	914	909	898	908	644	758
	M_{O_2}	0.13	0.07	0.03	0.02	0.21	0.05
Supported cluster	r_{O-O}	1.50	1.46	1.32	1.45	1.34	1.40
	ν_{O-O}	680	925	1164	938	1099	831
	M_{O_2}	0.00	0.09	0.01	0.00	0.77	0.22
Surface site	r_{O-O}	1.45	1.45	1.41	1.45	1.41	1.45
	ν_{O-O}	951	962	934	957	931	960
	M_{O_2}	0.00	0.00	0.00	0.00	0.00	0.02
Interface site	r_{O-O}	—	—	1.41	1.39	1.41	1.40
	ν_{O-O}	—	—	881	893	843	837
	M_{O_2}	—	—	0.04	0.00	0.02	0.00

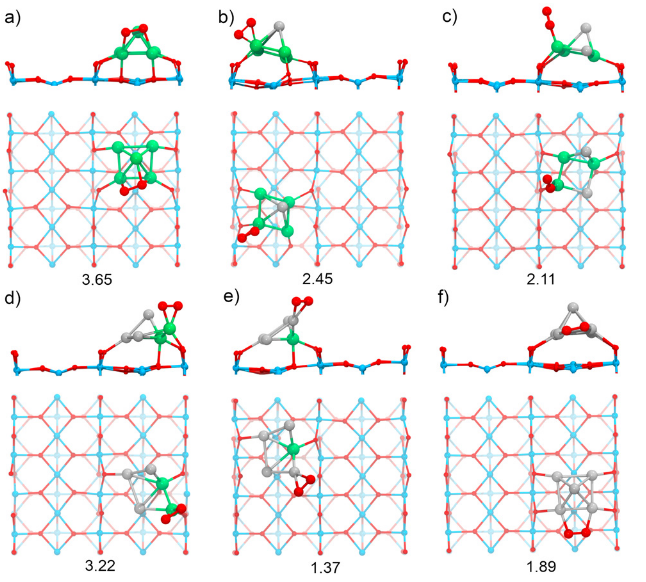

Fig. 5 The most stable structures for O_2 adsorption on Re_nPt_m ($n + m = 5$) clusters supported on $TiO_2(110)$ (Side and top views are displayed): (a) Re_5, (b) Re_4Pt_1, (c) Re_3Pt_2, (d) Re_2Pt_3, (e) Re_1Pt_4, (f) Pt_5. The adsorption energy (E_{ads}) is displayed below each structure in eV. For ease of analysis, only the last layer is shown in the simplified side view of the supported clusters.

for clusters in the gas phase, we find a clear trend for higher O_2 adsorption energies in the case of clusters with a high concentration of Re, whereas Pt_5 and Re_1Pt_4 clusters have much lower adsorption energies. The most stable adsorption modes on the supported clusters are: mono (η^1-Re), top (η^2-Pt, η^2-Re), and bridge (μ_3-Re, μ_2-Pt) types. The high fluxionality of the supported clusters results in important structural changes taking place upon adsorption of the O_2 molecule. This effect is particularly strong for the Re_3Pt_2 and Re_2Pt_3 clusters, where the Re atom that interacts with O_2 experiences a significant displacement, and the square pyramid distorts into a more open conformation. The O_2 on supported Re_nPt_m clusters has a bond length from 1.32 to 1.50 Å, a stretching frequency between 680 and 1164 cm^{-1}, and a magnetic moment from 0.00 to 0.77μ_B (see Table 1, which reports all the parameters for the adsorbing O_2 molecule in gas-phase and TiO_2 -supported clusters). These parameters can be related to superoxo (for Re_3Pt_2 and Re_1Pt_4) and peroxo species (for the rest of clusters), with the highest O–O bond activation taking place on Re_5, Re_4Pt_1, and Re_2Pt_3 clusters, consistent with the highest adsorption energies.

The Bader charge analysis was performed on the most stable structures to understand the activation of O_2 on gas-phase and supported Re_nPt_m clusters. Previous theoretical studies have shown that the charge transfer from the cluster to O_2 depends on the adsorption mode.[55,72] Fig. 6 shows the relationship between the charge received by O_2 and the O–O bond length, with the data labeled according to the adsorption mode. There is a linear relationship between the charge and bond length of O_2, with only the η^1-Re and μ_2-RePt modes showing some sizable discrepancies from the linear dependency. The O_2 molecule receives a charge ranging from 0.44 to 0.99 e, with the sites which transfer the largest amount of charge being Re atoms (cyan, green), results which are consistent with the larger intrinsic reactivity of these sites. The μ_3-Re and η^2-Re adsorption modes exhibited a magnetic moment of O_2 close to zero, suggesting a full occupation of the π^* antibonding orbitals of the molecule. In contrast, when O_2 adsorbs on Pt atoms charge transfer decreases and the magnetic moment increases, a fact which correlates with the lower adsorption energies at those sites. Therefore, charge transfer on O_2 gives a good measure of the activation of the O–O bond.

An analysis was conducted on the charge of the supported clusters both before and after O_2 adsorption, as well as the charge of each atom within the cluster (ESI,† Table S1). After adsorption of O_2, the total positive charge on the Re–Pt clusters increases as a result of the charge transfer to the oxygen molecule. Also, we find that the metal atoms directly bonded to O_2 are the ones who transfer the majority of the electronic charge to the oxygen molecule. The larger intrinsic reactivity of the Re atoms results in larger charge transfers, compared to Pt.

In Fig. 6b, we have also analyzed the PDOS for O_2 adsorption on supported Re_5 and Re_1Pt_4, which are the two clusters with the highest and lowest O_2 binding energy, respectively. The first panel shows the PDOS of gas-phase O_2, and the two panels below show the PDOS for these two supported clusters. For gas-phase O_2, the π^* antibonding orbitals split into occupied spin-up and unoccupied spin-down states, resulting in a triplet spin state and a magnetic moment of $2\mu_B$. Once the half-occupied π^* orbitals are filled, the spin splitting and the magnetic moment disappear.[73] When O_2 adsorbs at the supported clusters, there are significant differences between the Re-rich and Pt-rich cases. During the adsorption process the 2p-states of the molecule overlap with the 5d-states of the metal atoms, leading to chemisorption of O_2. In the case of Re_1Pt_4, the O_2 states of retain spin splitting and have a DOS similar to the superoxo species,[74] with antibonding π^* orbitals being unoccupied just above the Fermi level. For the Re_5 cluster the π^* antibonding orbitals are fully occupied, and become symmetric for spin up

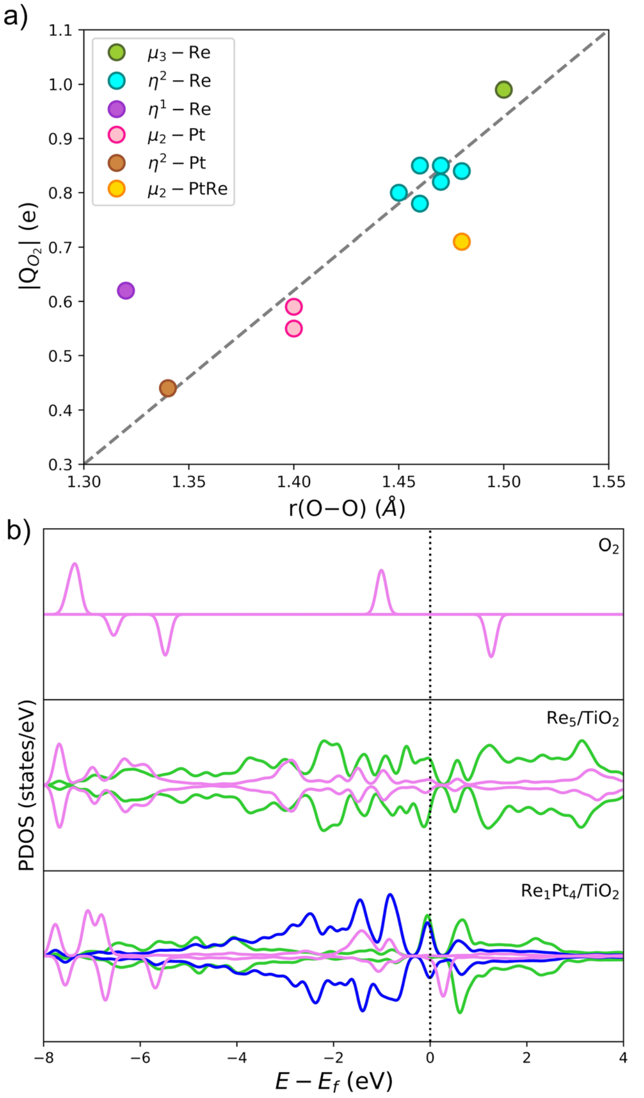

Fig. 6 Electronic properties for O_2 activation on metal cluster sites. (a) Relationship between O_2 charge and O–O length for O_2 adsorption on Re_nPt_m systems. These data correspond to the most stable sites on the gas-phase and supported clusters. (b) The projected density of states (PDOS) of the O_2 adsorption on Re_5 and Re_1Pt_4 supported clusters. The first panel shows the PDOS of gas-phase O_2, and the two panels below are the PDOS for the systems with higher and lower adsorption energy. The 5d states of Re, 5d states of Pt, and 2p states of O_2 are represented by green, blue, and pink, respectively.

and spin down, consistent with a peroxo state with the magnetic moment equal to zero. This comparison of the electronic structure for both compositions correlates with the larger cluster-O_2 charge transfer and much higher adsorption energy in the case of the Re-rich stoichiometry.

Next, we studied the dissociation of O_2 over the metal clusters, comparing the results for both gas-phase clusters, and clusters supported on TiO_2(110). In each case, the starting point for the dissociation was taken from the most stable site of molecular O_2 adsorption. Table 2 summarizes all the results, showing the values of the activation energies E_{act}, the reaction energies ΔE and the imaginary frequencies of the transition states, for both gas-phase and supported clusters. The reaction energies ΔE are defined as the energy difference between the initial state (with molecular O_2 bonded to the cluster) and the final state (with two separated O adatoms). For unsupported clusters, reaction energies are always large, of the order or 3 eV, with the sole exception of the pure Pt_5 cluster. This means that oxygen dissociation is highly exothermic, and dissociative adsorption is strongly favoured whenever there is at least one reactive Re atom in the cluster. In the absence of reactive Re atoms, the reaction energy for Pt_5 decreases to only −0.44 eV. Additionally, we calculated the free energy for the dissociation reaction at 300 K and 1 atm on Re_nPt_m ($n + m = 5$) gas-phase clusters (see data in Table S4 of the ESI†). In most cases, the thermal correction contributes less than 0.1 eV to the reaction energy. Thus, we observed that the trends remain consistent when considering the free energy at 300 K. Thus, this correction has no impact on our analysis.

Table 2 The activation barriers (E_{act}, eV), the reaction energies (ΔE, eV), and imaginary frequencies of the transition states (ν_i, cm^{-1}) for the dissociation of O_2 on the metal cluster site of gas- and supported-phases. In the gas-phase Re_5 cluster, the reaction path exhibits a continuously decreasing energy, resulting in the absence of a transition state (TS)

	Gas-phase clusters			Supported clusters		
	E_{act}	ΔE	ν_i	E_{act}	ΔE	ν_i
Re_5	—	−3.52	—	0.02	−2.92	415
Re_4Pt_1	0.41	−3.23	561	0.98	−3.25	224
Re_3Pt_2	0.18	−2.87	598	0.37	−3.43	216
Re_2Pt_3	0.53	−2.87	789	0.60	−3.10	579
Re_1Pt_4	0.05	−2.83	347	0.47	−1.41	136
Pt_5	0.24	−0.44	254	0.61	−0.18	174

For gas-phase clusters, the reaction path for O_2 dissociation is shown in Fig. 7. In all cases, activation barriers are low, in the range of 0.0–0.5 eV. The low value of the barrier and the large energy gain for dissociation of O_2 causes that, in general, the transition state was found for very small expansions of the O–O bond. In the case of pure Re_5, the barrier is extremely small, virtually non existent, and we were not able to properly identify a transition state. The corresponding results for clusters supported on the TiO_2(110) surface are shown in Fig. 8. Activation barriers are slightly larger, although they never exceed 1 eV. Again, dissociation of O_2 on pure Re_5 takes place almost spontaneously, with only a residual barrier of 0.02 eV. The interaction of the surface with the cluster causes some important changes in the mechanisms for O_2 dissociation for some compositions; for pure Pt_5, the supported cluster undergoes a drastic configuration change after oxygen dissociation and loses bonds at the metal-substrate interface. Reaction energies for supported clusters are, in general, similar to the ones found for gas-phase cluster, with one very important exception, the Re_1Pt_4 cluster. When this cluster is supported, the reaction energy drops from 2.8 to 1.4 eV. This effect is caused by the binding of the Re atom to the substrate, which serves as an anchoring point. Since this atom is unaccessible to the adsorbed O_2 molecule (as there are several Pt atoms on top of it), dissociation must take place at less reactive Pt sites, with an

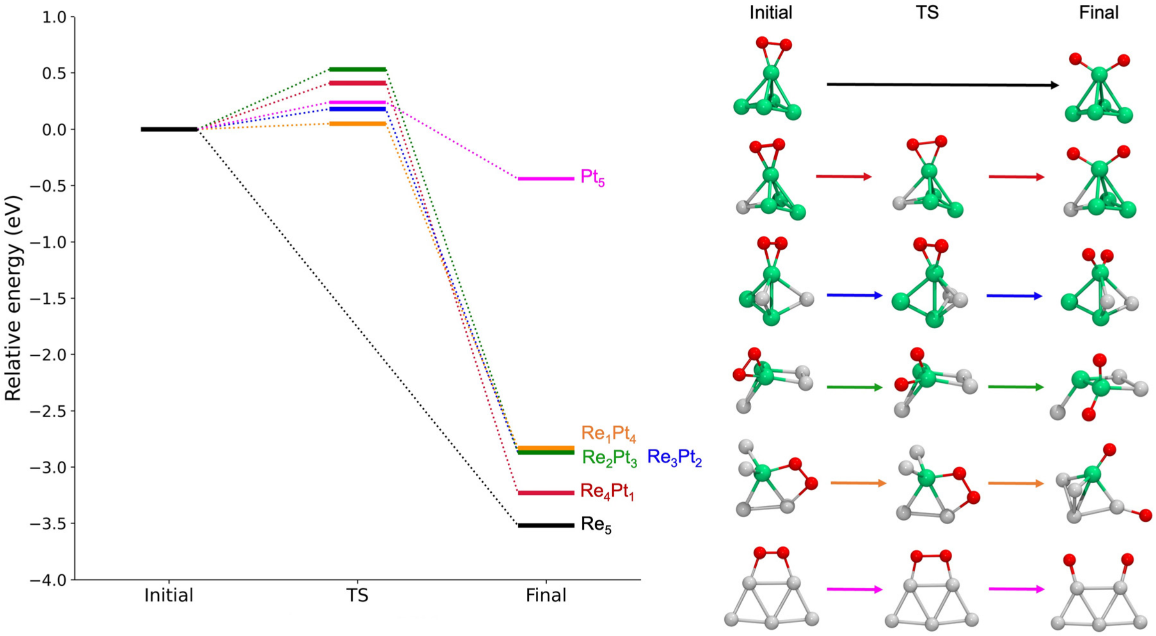

Fig. 7 Left panel: Reaction energetics for the dissociation of O_2 on gas-phase Re_nPt_m clusters. All the energies are shown relative to the one of the initial state, on each case. Right panel: Structures for initial, transition and final states for each cluster. The colors of the atoms are consistent with those in previous figures.

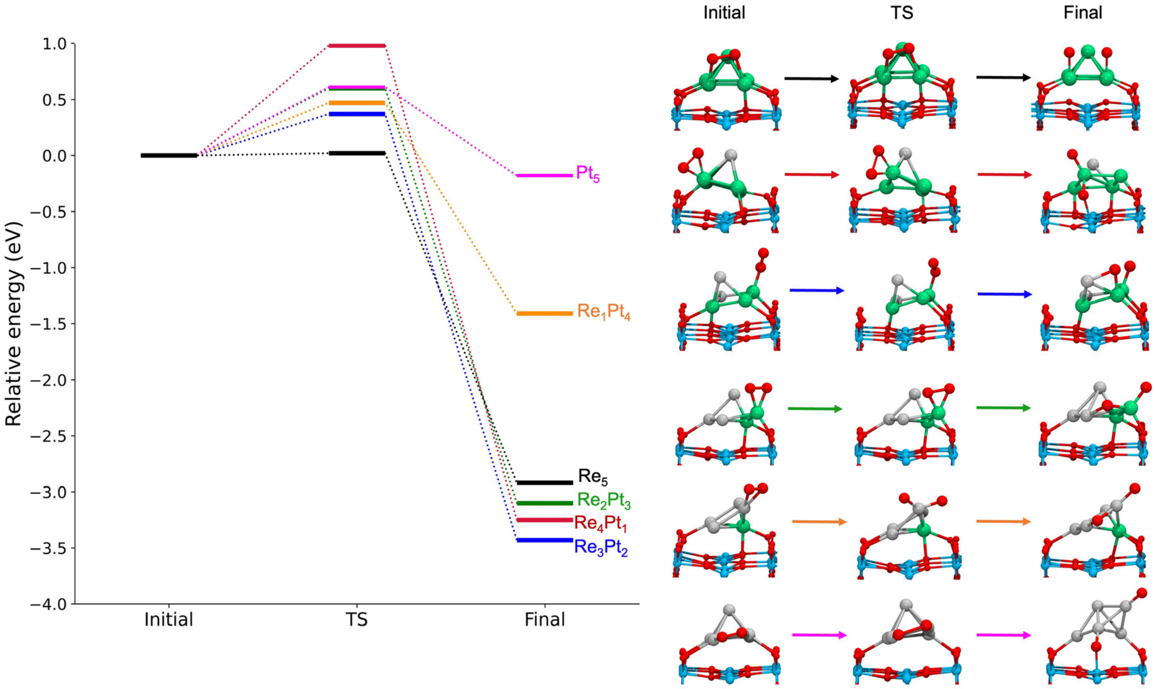

Fig. 8 Left panel: Reaction energetics for the dissociation of O_2 on supported Re_nPt_m clusters. All the energies are shown relative to the one of the initial state, on each case. Right panel: Structures for initial, transition and final states for each cluster. The colors of the atoms are consistent with those in previous figures.

important energetic cost. Overall, the results show that for all compositions dissociation of O_2 is an exothermic process with low activation barriers. Nevertheless, there are important quantitative differences between Re-rich clusters, much more reactive, and Pt-rich ones; whenever the reactive Re sites are not available, sizable changes in reactivity will occur.

We have analyzed the charge transfer to O_2 when it adsorbs on TiO_2-supported clusters (see data in Table S3 of the ESI†). In all the cases, almost all the charge is donated from the 5d-states of the metal clusters, with the change donated from the TiO_2 substrate being very small. Finally, we also studied the most stable conformations for the two dissociated oxygen adatoms on both gas-phase and supported clusters. The results are shown in Fig. S4 of the ESI.† In many cases, diffusion of oxygen atoms towards more stable locations is linked to strong conformational changes in the cluster. This happens both for unsupported and for supported clusters. Also, it must be noted that, with respect to the final states reported on Fig. 8, there is a consistent tendency towards separation of the oxygen adatoms; initially, these are bonded to the same atom, but a large energy gain takes place when each one binds at a separate metal site.

3.3 Adsorption of O_2 to surface sites of TiO_2 substrate

We will now study the adsorption of O_2 to surface sites of the TiO_2 substrate, separated some distance from Re_nPt_m clusters previously deposited on the surface. First, we have checked that on the pristine TiO_2 surface (that is, without metal clusters supported on it) O_2 adsorption is very weak (E_{ads} = 0.11 eV), which is in agreement with other theoretical studies.[37,75] On the contrary, Sokolovic *et al.* reported that the reduced TiO_2(110) surface can adsorb the oxygen molecule.[76] The presence of oxygen vacancies leads to the formation of small polarons located on the next-nearest subsurface Ti_{6c} atoms. These polarons transfer charge to the adsorbed O_2 molecule, resulting in the formation of the peroxo species and atomic oxygen.[76]

Similar to the case of reduced TiO_2(110) surface with oxygen vacancies, the pristine TiO_2 surface with Re_nPt_m clusters supported on it also contains small surface polarons. Previously, our analysis of the electronic structure of the Re_nPt_m/TiO_2(110) system has shown that the metal clusters transfer electrons to the surface, leading effectively to the reduction of Ti_{5c} atoms. Consequently, we find that in the presence of supported metal clusters the O_2 can adsorb on surface Ti_{5c} with moderately strong adsorption energies, ranging from 0.93 to 1.55 eV (ESI,† Table S2). In general, adsorption of O_2 is slightly stronger in the case of Re-rich clusters; the stronger cluster–surface interaction and larger charge transfer also results in stronger O_2–TiO_2 interactions. In the case of supported Pt_5 and Re_1Pt_4, the adsorption energies of O_2 on the surface Ti_{5c} sites are comparable to the ones obtained when O_2 adsorbs at these clusters. This means that O_2 adsorption on the surface may be significant for these compositions. Also, the process of O_2 spillover from the supported cluster to the substrate is feasible, given the similar stability of molecular O_2 at both sites. In contrast, for Re-rich compositions, the adsorption energy of O_2 is much higher at the metal sites. This fact, together with the very high reaction energy for O_2 dissociation at the Re-rich clusters, implies that any O_2 molecule that could diffuse from surface sites to the cluster will remain there, being dissociated afterwards.

Depending on the cluster composition, we found two competing adsorption modes: a η^2-Ti mode which displaces vertically the Ti_{5c} atom from the surface by about 1 Å, and a μ_2-Ti mode where O_2 bridges two surface Ti_{5c} sites, with very small vertical displacements for both Ti_{5c} sites. Fig. 9 shows the relaxed structures for these adsorption modes, for the supported Re_1Pt_4 and Pt_5 clusters. The O–O bond lengths for each of these two modes are 1.45 and 1.41 Å, respectively (see Table 1). The stretching frequency for the adsorbed O_2 molecule ranges from 931 to 962 cm^{-1}, and its magnetic moment is always equal to zero. These facts indicate that the O_2 molecule adsorbs to Ti_{5c} surface sites as a peroxo species.

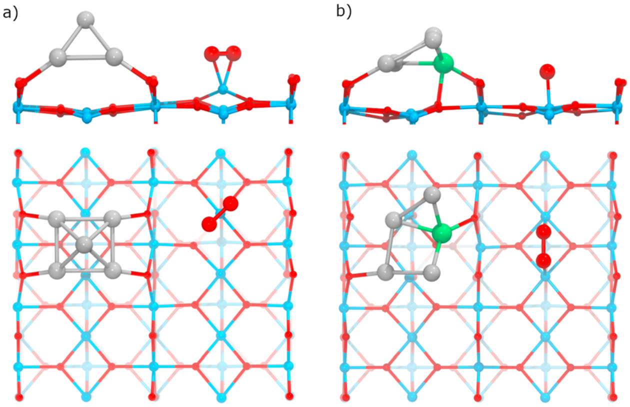

Fig. 9 Relaxed structures for O_2 adsorption on the TiO_2(110) surface in the presence of supported Re_nPt_m clusters. (a) The η^2-Ti mode on the surface site (Pt_5 supported system). (b) The μ_2-Ti mode on the surface site (Re_1Pt_4 supported system).

We have also analyzed the electronic structure of molecular O_2 adsorbed at Ti_{5c} surface sites. Table S3 in the ESI† shows the charge transfer to the O_2 molecule, for each of the co-adsorbed Re_nPt_m clusters. The values are fairly uniform, ranging from 0.88 to 0.94 electrons. It is interesting to compare the results for O_2 adsorption to the metal atoms of the cluster with adsorption of O_2 at surface Ti_{5c} sites. When O_2 adsorbs at the TiO_2 substrate, some part of the charge donated to oxygen is transferred from the substrate, and other part from the cluster. Interestingly, the amount of charge transferred from the surface decreases as the amount of Pt in the cluster increases. We also calculated the PDOS of bimetallic Re–Pt clusters after the O_2 adsorption on the surface and analyzed the electronic states of the reduced Ti atoms in the substrate. To enhance the clarity of the plots, we multiplied the Ti^{3+}, the O_2 molecule and metal clusters states by ten in the PDOS (Fig. 10). The 5d-states of Pt and Re exhibit minor changes because they do not participate directly on the O_2 bonding. The displayed states only show spin up as there is no spin splitting. The 3d states of Ti^{3+} for Re_3Pt_2 and Re_1Pt_4 systems disappear, indicating a charge transfer from Ti^{3+} atoms to the O_2 molecule. Although the other systems retain some polaronic states, there is a significant reduction. This was verified by analyzing the magnetic moment of the Ti atoms, where only one or no polaron remains after adsorption. Thus, Ti^{3+} atoms facilitate the adsorption of O_2 on the surface by transferring electrons to the molecule.

Finally, we have considered the possibility of dissociation of the O_2 molecule adsorbed at Ti_{5c} surface sites. The results in Fig. 10b show that this is a very endothermic process. Barriers

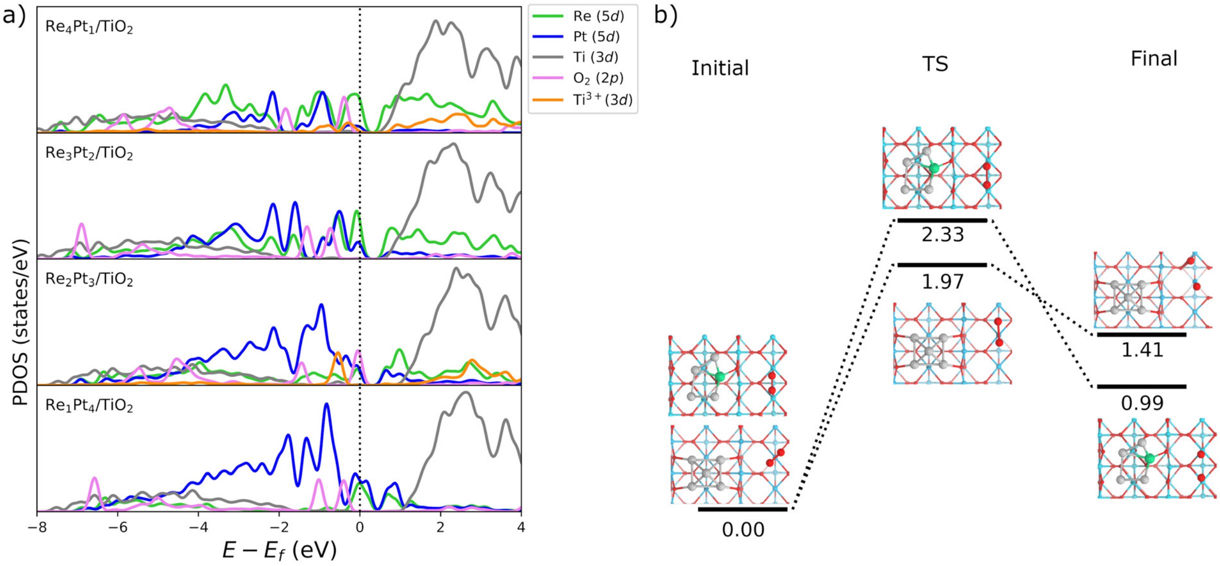

Fig. 10 (a) Projected density of states (PDOS) for O_2 adsorbed on the $TiO_2(110)$ surface in the presence of supported Re_nPt_m clusters. The 5d states of Re, 5d states of Pt, 3d states of Ti^{4+}, 3d states of Ti^{3+}, and 2p states of O_2 are represented by green, blue, gray, orange, and pink, respectively. The Ti^{3+}, the O_2 molecule, and metal clusters states are multiplied by ten in the PDOS. (b) Energetic barriers for the dissociation of O_2 on $TiO_2(110)$ surface in the presence of supported Pt_5 and Re_1Pt_4 clusters.

for O_2 dissociation on the surface were calculated in the case of coadsorbed Pt_5 and Re_1Pt_4 systems. In both cases, energy barriers are very high (1.97 and 2.33 eV), leading to final states at least 1 eV higher in energy than the initial state with the O_2 molecule intact. This contrasts with the experimental observation of atomic oxygen on the surface with oxygen vacancies.[76] Therefore, on surface sites around the Re–Pt supported clusters O_2 only experiments a mild activation to a peroxo state, with complete dissociation being unfeasible due to the large barriers involved.

3.4 Adsorption and activation of O_2 by the metal-support interface

Finally, we have investigated the adsorption and dissociation of O_2 at interfacial cluster-TiO_2 sites, with the O_2 molecule forming bonds with both Ti_{5c} surface atoms and Pt or Re atoms in the supported cluster. These types of catalytic sites are extremely important for a variety of systems and reactions. On one hand, stability of adsorbates at these locations determines if processes of spillover from the cluster to the substrate are feasible (or conversely, reverse spillover from the substrate to the cluster). On the other hand, these sites are the natural meeting place for different reactants which prefer to bind either at the supported cluster, or at the substrate. As a consequence, for many oxidation reactions these sites are believed to be the active sites where the reaction takes place.[77,78] Fig. 11a shows the most stable conformations found for molecular O_2 adsorbed at the cluster-support interface for Re_3Pt_2, Re_2Pt_3, Re_1Pt_4, and Pt_5 clusters. For all these compositions, the molecule adsorbs bridging a Ti_{5c} atom in the surface and a Pt atom within the cluster. For Re_5 and Re_4Pt_1, the cluster-support interface is composed exclusively by Re atoms. In these cases, when we relaxed initial starting geometries with O_2 bridging Ti and Re sites, we found that the O_2 molecule spontaneously dissociates into an oxygen atom bonded to the Re sites in the cluster and another oxygen atom which remains bonded to the Ti_{5c} surface site (see Fig. S5 in the ESI†). It is interesting to compare the binding energies of the final states with one O atom adsorbed at the substrate (4.43 and 5.12 eV for Re_5 and Re_4Pt_1, respectively) with the corresponding values where the two oxygen adatoms remain bonded to the Re-rich clusters (7.74 and 6.65 eV for the most stable conformations on each case). Clearly, there is a high energetic cost against spillover of dissociated oxygen atoms to the substrate, in the case of Re-rich clusters.

The adsorption energies at Pt sites vary in a range between 1.41 to 2.05 eV. Such binding strength is similar to the values found for O_2 bound at the supported Pt-rich clusters, and it is only slightly larger than the values found at the Ti_{5c} surface sites away from the cluster. The most stable adsorption modes are μ_2-TiPt and μ_3-TiPt with O–O length ranging from 1.39 to 1.41 Å. At the interface, O_2 has a stretching frequency varying between 837 and 893 cm^{-1}, and a magnetic moment equal to zero (see Table 1). Therefore, adsorption of O_2 at these sites takes place as a peroxo species. The charge transfer to the O_2 molecule if fairly constant, between −0.83 and −0.88 electrons. Part of this extra charge is transferred from the substrate, but the majority is donated by the supported cluster (see Table S3 in the ESI†).

Finally, we have calculated the energy barriers for O_2 dissociation at the interface of supported Pt-rich clusters (Pt_5 and Re_1Pt_4, see Fig. 11b). We find that oxygen atom dissociates on the surface and the other on the Pt atoms of the cluster. The process is exothermic, and the energy barriers are similar to those found at the metal cluster site (less than 0.70 eV). Although Re does not directly participate in the dissociation

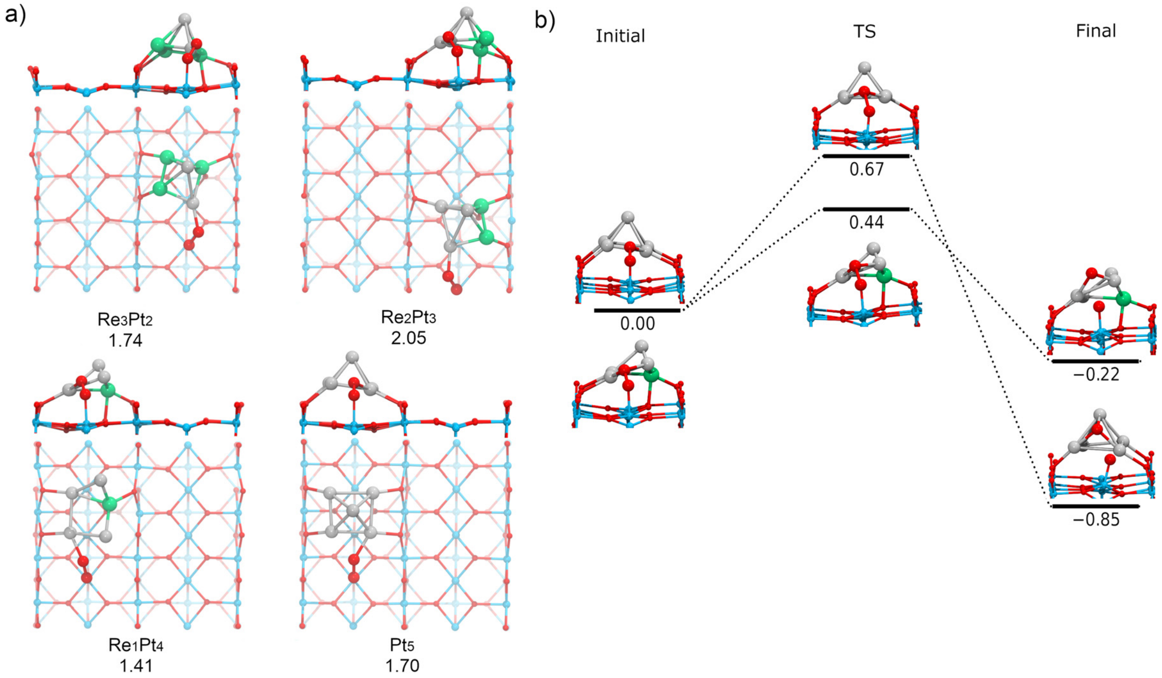

Fig. 11 O_2 adsorption on the Ti–Pt interface. (a) The most stable structures for O_2 adsorption on the interface of Re_3Pt_2, Re_2Pt_3, Re_1Pt_4, and Pt_5 supported clusters. The adsorption energy (E_{ads}) is displayed below each structure in eV. The structure of the supported clusters is simplified by showing only the surface trilayer for ease of analysis. (b) Energetic barriers to dissociation of O_2 on the Ti–Pt interface of Pt_5 and Re_1Pt_4 supported clusters.

of O_2 in this case, it can be observed that the dissociation barrier is lower for the cluster containing a Re impurity. Contrary to the case of Re-rich clusters, the energetic cost for transferring oxygen adatoms from the cluster to the TiO_2 substrate is not very high, which means that spillover of dissociated oxygen to the surface can take place for Pt-rich clusters. Overall, our results show that dissociation of O_2 at the Pt–Ti interface requires little energy, whereas the Re–Ti interface causes a dissociative adsorption of O_2, leading to spontaneous production of atomic oxygen.

4 Conclusions

In this study, the adsorption and activation of O_2 on Re_nPt_m ($n + m = 5$) clusters, both free and supported on $TiO_2(110)$, were investigated at the metal cluster, surface, and interfacial sites. The most stable structures for the supported clusters, at various compositions, are characterized by a strong tendency for the Re atoms in the cluster to occupy positions directly in contact with the oxygen surface sites; therefore, in mixed Pt–Re clusters it is expected that Pt atoms will preferentially be displaced towards the top part of the supported cluster, while Re accumulates at the interfacial area, increasing the adhesion of the cluster to the substrate. The composition of Re_nPt_m clusters can tune the formation of surface polarons, increasing the reactivity of the surface towards reactions involving charge transfer. Thus, changes in reactivity may occur due to alterations in the cluster and surface, resulting in the emergence of new active sites, including those found at the interface and on the reduced surface. At the metal cluster sites, the Re_nPt_m clusters have a strong interaction with the O_2 molecule, especially on the Re atoms, which are much more reactive than the Pt atoms. The O_2 molecule adsorbed on Re–Pt clusters exhibits parameters typical of the peroxo species. This activation of the O–O bond is caused by charge transfer from the cluster atoms to the molecule. Dissociative adsorption can occur on Re atoms due to their significant charge donation to O_2. In general, oxidation is expected in Re_nPt_m ($n + m = 5$) clusters because the energy barriers for dissociation are low (less than 0.7 eV). Finally, the bimetallic Re_1Pt_4 cluster exhibits a synergistic effect of the metal atoms on its stability and reactivity. The cluster is anchored on the surface by the Re atom, while the Pt atoms activate the O_2 molecule.

At the surface sites, the composition of Re_nPt_m clusters can tune the formation of surface polarons. Re-rich clusters transfer more electrons to the $TiO_2(110)$ surface than Pt-rich clusters, resulting in increased surface reactivity. The oxygen molecule adsorbs onto Ti atoms with moderate adsorption energies (0.93–1.55 eV). The electronic and structural parameters displayed by the O_2 on the surface site are analogous to those of peroxo species. Due to the adsorption of oxygen, certain polarons disappear, indicating their involvement in the activation process. However, the activation of O_2 can be considered mild on the surface site of Re–Pt supported clusters due to the high energy requirement to break the O–O bond. This finding contrasts with experimental reports for the $TiO_2(110)$ surface with oxygen vacancies, where atomic oxygen has been observed.

At the interfacial cluster-support sites, the Re–Ti interface causes the dissociative adsorption of O_2, while the Pt–Ti interface activates the O_2 molecule with typical structural parameters of a peroxo species. At the Pt–Ti interface, the adsorption energies show a slight increase with respect to the surface sites. Other clusters also exhibit O_2 adsorption at the interface, such as Au clusters on the MgO(100)[79] and $TiO_2(101)$[80] surfaces. Both the metal cluster and Ti surface atoms transfer charge to the O_2 molecule. The energy barriers for the dissociation of O_2 at the Pt–Ti interface are low, similar to what was found for the cluster sites. Thus, in an oxidizing atmosphere, the interfaces of Pt/TiO_2 and Re/TiO_2 may become enriched with atomic oxygen. The interface can be an active site for chemical reactions, especially for oxidation reactions that require O_2 activation.[77]

In summary, the Re_nPt_m ($n + m = 5$) clusters supported on $TiO_2(110)$ display three possible sites for O_2 adsorption: the metal cluster, the surface, and the interface. All sites transfer charge to the O_2 molecule and elongate the O–O bond. In these supported clusters, the metal cluster and interface sites can dissociate the O_2 molecule with low energy requirements, while the surface sites requires much more energy. Thus, the sites containing Re and Pt atoms, as well as the Re–Ti and Pt–Ti interfaces, are expected to be oxidized. In Re_1Pt_4 and Pt_5 supported systems, the three active sites compete with each other due to their similar adsorption energies. In terms of the role of metal atoms, Re serves to anchor the cluster to the surface, while Pt is more available to interact with O_2. These findings provide new insight into the activation of O_2 on Re–Pt clusters supported on $TiO_2(110)$ as single-cluster catalysts.

Author contributions

Conceptualisation: AAG, ILG, LMM; formal analysis: AAG, ILG, LMM; funding acquisition: ILG, LMM; supervision: ILG, LMM; visualisation: AAG; writing – original draft: AAG; writing – review & editing: ILG, LMM.

Conflicts of interest

There are no conflicts to declare.

Acknowledgements

Andrés Álvarez-García gratefully thanks CONACyT-Mexico for the PhD scholarship No. 957475. Calculations were performed at the DGTIC-UNAM Supercomputing Center under Project LANCAD-UNAM-DGTIC-049. This work was supported by DGAPA-UNAM PAPIIT under Project IN106021 and CONACyT-Mexico under Project 285821. Luis M. Molina acknowledges the support from Ministerio de Ciencia e Innovación of Spain (Grant PID2022-138340OB-I00 funded by MCIN/AEI/10.13039/501100011033 and FSE +) and from the University of Valladolid (GIR Nanostructure Physics).

Notes and references

1 C. Dong, Y. Li, D. Cheng, M. Zhang, J. Liu, Y.-G. Wang, D. Xiao and D. Ma, *ACS Catal.*, 2020, **10**, 11011–11045.

2 A. J. Brandt, T. D. Maddumapatabandi, D. M. Shakya, K. Xie, G. S. Seuser, S. Farzandh and D. A. Chen, *J. Chem. Phys.*, 2019, **151**, 234714.

3 R. P. Galhenage, K. Xie, H. Yan, G. S. Seuser and D. A. Chen, *J. Phys. Chem. C*, 2016, **120**, 10866–10878.

4 A. S. Duke, R. P. Galhenage, S. A. Tenney, P. Sutter and D. A. Chen, *J. Phys. Chem. C*, 2015, **119**, 381–391.

5 K. Tomishige, Y. Nakagawa and M. Tamura, *Chin. Chem. Lett.*, 2020, **31**, 1071–1077.

6 J. Xiao and R. J. Puddephatt, *Coord. Chem. Rev.*, 1995, **143**, 457–500.

7 A. S. Duke, K. Xie, A. J. Brandt, T. D. Maddumapatabandi, S. C. Ammal, A. Heyden, J. R. Monnier and D. A. Chen, *ACS Catal.*, 2017, **7**, 2597–2606.

8 A. S. Duke, K. Xie, A. J. Brandt, T. D. Maddumapatabandi, S. C. Ammal, A. Heyden, J. R. Monnier and D. A. Chen, *ACS Catal.*, 2017, **7**, 2597–2606.

9 L. Kang, B. Wang, Q. Bing, M. Zalibera, R. Büchel, R. Xu, Q. Wang, Y. Liu, D. Gianolio, C. C. Tang, E. K. Gibson, M. Danaie, C. Allen, K. Wu, S. Marlow, L. D. Sun, Q. He, S. Guan, A. Savitsky, J. J. Velasco-Vélez, J. Callison, C. W. Kay, S. E. Pratsinis, W. Lubitz, J. Y. Liu and F. R. Wang, *Nat. Commun.*, 2020, **11**, 17–19.

10 L. X. Chen, Z. Wen, Z. W. Chen, C. V. Singh and Q. Jiang, *J. Mater. Chem. A*, 2021, **9**, 11726–11733.

11 C. Vogt and B. M. Weckhuysen, *Nat. Rev. Chem.*, 2022, **6**, 89–111.

12 S. Dai, J. P. Chou, K. W. Wang, Y. Y. Hsu, A. Hu, X. Pan and T. Y. Chen, *Nat. Commun.*, 2019, **10**, 1–10.

13 A. Trinchero, S. Klacar, L. O. Paz-Borbón, A. Hellman and H. Grönbeck, *J. Phys. Chem. C*, 2015, **119**, 10797–10803.

14 M. M. Montemore, M. A. Van Spronsen, R. J. Madix and C. M. Friend, *Chem. Rev.*, 2018, **118**, 2816–2862.

15 X. Li, S. Mitchell, Y. Fang, J. Li, J. Perez-Ramirez and J. Lu, *Nat. Rev. Chem.*, 2023, 754–767.

16 S. Vajda, M. J. Pellin, J. P. Greeley, C. L. Marshall, L. A. Curtiss, G. A. Ballentine, J. W. Elam, S. Catillon-mucherie, P. C. Redfern, F. Mehmood and P. Zapol, *Nat. Mater.*, 2009, **8**, 213–216.

17 L. Liu and A. Corma, *Chem. Rev.*, 2018, **118**, 4981–5079.

18 S. Baskaran, C. Q. Xu, Y. G. Wang, I. L. Garzón and J. Li, *Sci. China Mater.*, 2020, **63**, 993–1002.

19 Y. Watanabe, *Sci. Technol. Adv. Mater.*, 2014, **15**, 1–12.

20 B. Ni and X. Wang, *Chem. Sci.*, 2016, **7**, 3978–3991.

21 C. Yao, N. Guo, S. Xi, C. Q. Xu, W. Liu, X. Zhao, J. Li, H. Fang, J. Su, Z. Chen, H. Yan, Z. Qiu, P. Lyu, C. Chen, H. Xu, X. Peng, X. Li, B. Liu, C. Su, S. J. Pennycook, C. J. Sun, J. Li, C. Zhang, Y. Du and J. Lu, *Nat. Commun.*, 2020, **11**, 4389.

22 X. L. Ma, J. C. Liu, H. Xiao and J. Li, *J. Am. Chem. Soc.*, 2018, **140**, 46–49.

23 S. Vajda and M. G. White, *ACS Catal.*, 2015, **5**, 7152–7176.

24 P. Kaghazchi and T. Jacob, *Phys. Rev. B: Condens. Matter Mater. Phys.*, 2011, **83**, 035417.
25 Y.-K. Jeong, Y. M. Lee, J. Yun, T. Mazur, M. Kim, Y. J. Kim, M. Dygas, S. H. Choi, K. S. Kim, O.-H. Kwon, S. M. Yoon and B. A. Grzybowski, *J. Am. Chem. Soc.*, 2017, **139**, 15088–15093.
26 A. S. Chaves, G. G. Rondina, M. J. Piotrowski, P. Tereshchuk and J. L. F. Da Silva, *J. Phys. Chem. A*, 2014, **118**, 10813–10821.
27 O. Miramontes, F. Bonafé, U. Santiago, E. Larios-Rodriguez, J. J. Velázquez-Salazar, M. M. Mariscal and M. J. Yacaman, *Phys. Chem. Chem. Phys.*, 2015, **17**, 7898–7906.
28 N. Isomura, X. Wu and Y. Watanabe, *J. Chem. Phys.*, 2009, **131**, 164707.
29 S. Bonanni, K. Aït-Mansour, W. Harbich and H. Brune, *J. Am. Chem. Soc.*, 2012, **134**, 3445–3450.
30 A. Álvarez-García, J. C. Luque-Ceballos, L. O. Paz-Borbón and I. L. Garzón, *Comput. Mater. Sci.*, 2022, **214**, 111697.
31 S. Huseyinova, J. Blanco, F. G. Requejo, J. M. Ramallo-López, M. C. Blanco, D. Buceta and M. A. López-Quintela, *J. Phys. Chem. C*, 2016, **120**, 15902–15908.
32 A. R. Puigdollers, P. Schlexer, S. Tosoni and G. Pacchioni, *ACS Catal.*, 2017, **7**, 6493–6513.
33 P. G. Moses, A. Janotti, C. Franchini, G. Kresse and C. G. Van De Walle, *J. Appl. Phys.*, 2016, **119**, 181503.
34 L. O. Paz-Borbón, A. López-Martínez, I. L. Garzón, A. Posada-Amarillas and H. Grönbeck, *Phys. Chem. Chem. Phys.*, 2017, **19**, 17845–17855.
35 H. F. Wen, H. Sang, Y. Sugawara and Y. J. Li, *Phys. Chem. Chem. Phys.*, 2020, **22**, 19795–19801.
36 H. Xu and S. Y. Tong, *Surf. Sci.*, 2013, **610**, 33–41.
37 L. M. Liu, P. Crawford and P. Hu, *Prog. Surf. Sci.*, 2009, **84**, 155–176.
38 R. Y. Wang, J. X. Wang, J. Jia and H. S. Wu, *Appl. Surf. Sci.*, 2021, **536**, 147793.
39 C. Franchini, M. Reticcioli, M. Setvin and U. Diebold, *Nat. Rev. Mater.*, 2021, **6**, 560–586.
40 J. R. D. Lile, A. Bahadoran, S. Zhou and J. Zhang, *Adv. Theory Simul.*, 2022, **5**, 2100244.
41 M. Pilar de Lara-Castells, A. W. Hauser, J. M. Ramallo-López, D. Buceta, L. J. Giovanetti, M. A. López-Quintela and F. G. Requejo, *J. Mater. Chem. A*, 2019, **7**, 7489–7500.
42 P. López-Caballero, S. Miret-Artés, A. O. Mitrushchenkov and M. P. De Lara-Castells, *J. Chem. Phys.*, 2020, **153**, 164702.
43 P. López-Caballero, J. M. Ramallo-López, L. J. Giovanetti, D. Buceta, S. Miret-Artés, M. A. López-Quintela, F. G. Requejo and M. P. D. Lara-Castells, *J. Mater. Chem. A*, 2020, **8**, 6842–6853.
44 F. R. Negreiros, E. Aprà, G. Barcaro, L. Sementa, S. Vajda and A. Fortunelli, *Nanoscale*, 2012, **4**, 1208–1219.
45 L. O. Paz-Borbón, F. Buendiá, I. L. Garzón, A. Posada-Amarillas, F. Illas and J. Li, *Phys. Chem. Chem. Phys.*, 2019, **21**, 15286–15296.
46 C. J. Heard, S. Heiles, S. Vajda and R. L. Johnston, *Nanoscale*, 2014, **6**, 11777–11788.
47 G. Kresse and J. Furthmüller, *Phys. Rev. B: Condens. Matter Mater. Phys.*, 1996, **54**, 11169–11186.
48 J. P. Perdew, K. Burke and M. Ernzerhof, *Phys. Rev. Lett.*, 1996, **77**, 3865–3868.
49 G. Kresse and D. Joubert, *Phys. Rev. B: Condens. Matter Mater. Phys.*, 1999, **59**, 1758–1775.
50 P. E. Blöchl, *Phys. Rev. B: Condens. Matter Mater. Phys.*, 1994, **50**, 17953–17979.
51 S. L. Dudarev, G. A. Botton, S. Y. Savrasov, C. J. Humphreys and A. P. Sutton, *Phys. Rev. B: Condens. Matter Mater. Phys.*, 1998, **57**, 1505–1509.
52 V. Ç. Çelik, H. Ünal, E. Mete and Ş. Ellialtıoğlu, *Phys. Rev. B: Condens. Matter Mater. Phys.*, 2010, **82**, 205113.
53 L. E. Gálvez-González, J. O. Juárez-Sánchez, R. Pacheco-Contreras, I. L. Garzón, L. O. Paz-Borbón and A. Posada-Amarillas, *Phys. Chem. Chem. Phys.*, 2018, **20**, 17071–17080.
54 E. Davari and D. G. Ivey, *Sustainable Energy Fuels*, 2018, **2**, 39–67.
55 E. Fernández, M. Boronat and A. Corma, *J. Phys. Chem. C*, 2015, **119**, 19832–19846.
56 M. Yu and D. R. Trinkle, *J. Chem. Phys.*, 2011, **134**, 064111.
57 W. Tang, E. Sanville and G. Henkelman, *J. Phys.: Condens. Matter*, 2009, **21**, 084204.
58 V. Wang, N. Xu, J.-C. Liu, G. Tang and W.-T. Geng, *Comput. Phys. Commun.*, 2021, **267**, 108033.
59 G. Henkelman, B. P. Uberuaga and H. Jónsson, *J. Chem. Phys.*, 2000, **113**, 9901–9904.
60 H. E. Sauceda, F. Salazar, L. A. Pérez and I. L. Garzón, *J. Phys. Chem. C*, 2013, **117**, 25160–25168.
61 A. Posada-Amarillas and I. L. Garzón, *Phys. Rev. B: Condens. Matter Mater. Phys.*, 1996, **54**, 10362.
62 J. Zhang and A. N. Alexandrova, *J. Phys. Chem. Lett.*, 2013, **4**, 2250–2255.
63 S. V. Ong and S. N. Khanna, *J. Phys. Chem. C*, 2012, **116**, 3105–3111.
64 D. E. Jiang, S. H. Overbury and S. Dai, *J. Phys. Chem. C*, 2012, **116**, 21880–21885.
65 Y. Wang and H. Gao, *J. Phys. Chem. B*, 2017, **121**, 2132–2141.
66 A. Álvarez-García, J. C. Luque-Ceballos, L. O. Paz-Borbón and I. L. Garzón, *Surf. Sci.*, 2023, **733**, 122287.
67 P. M. Kowalski, M. F. Camellone, N. N. Nair, B. Meyer and D. Marx, *Phys. Rev. Lett.*, 2010, **105**, 5–8.
68 T. Shibuya, K. Yasuoka, S. Mirbt and B. Sanyal, *J. Phys.: Condens. Matter*, 2012, **24**, 435504.
69 Q. Wu, S. Hou, D. Buceta, H. J. Ordoñez, M. Arturo López-Quintela and C. J. Lambert, *Appl. Surf. Sci.*, 2022, **594**, 153455.
70 G. Herzberg, *Molecular Spectra and Molecular Structure I: Spectra of Diatomic Molecules*, D. Van Nostran Company, 2nd edn, 1963, pp. 1–658.
71 R. Wang, L. Zhao, J. Jia and H. S. Wu, *AIP Adv.*, 2018, **8**, 035307.
72 M. Boronat, A. Pulido, P. Concepción and A. Corma, *Phys. Chem. Chem. Phys.*, 2014, **16**, 26600–26612.
73 P. P. Mkhonto, H. R. Chauke and P. E. Ngoepe, *Minerals*, 2015, **5**, 665–678.
74 M. Alducin, D. Sánchez-Portal, A. Arnau and N. Lorente, *Phys. Rev. Lett.*, 2010, **104**, 1–4.
75 Z. Dohnálek, J. Kim, O. Bondarchuk, J. M. White and B. D. Kay, *J. Phys. Chem. B*, 2006, **110**, 6229–6235.

76 I. Sokolovic, M. Reticcioli, M. Calkovsky, M. Wagner, M. Schmid, C. Franchini, U. Diebold and M. Setvín, *Proc. Natl. Acad. Sci. U. S. A.*, 2020, **117**, 14827–14837.

77 L. M. Molina and B. Hammer, *Phys. Rev. B: Condens. Matter Mater. Phys.*, 2004, **69**, 1–22.

78 L. B. Vilhelmsen and B. Hammer, *ACS Catal.*, 2014, **4**, 1626–1631.

79 Z. Duan and G. Henkelman, *Phys. Chem. Chem. Phys.*, 2016, **18**, 5486–5490.

80 J. Fabila, D. Romero, L. O. Paz-Borbón and F. Buendía, *J. Chem. Phys.*, 2022, **157**, 084309.